AIAA JOURNAL
Vol. 42, No. 11, November 2004

Wake of a Compressor Cascade with Tip Gap, Part 2: Effects of Endwall Motion

Yu Wang* and William J. Devenport†
Virginia Polytechnic Institute and State University, Blacksburg, Virginia 24061

The effects of relative motion between the blade tips and endwall on the flow downstream of a linear compressor cascade have been studied. Endwall motion was simulated by using a 0.25-mm-thick Mylar belt propelled over a sliding surface beneath the tips of the cascade blades. Three-component mean-velocity and turbulence measurements made in cross sections downstream of the cascade reveal that the wall motion flattens and shears the turbulence and mean-velocity distributions of the vortex. Mean-helicity density plots also show that endwall motion smears the vortex center from a single point (when seen in cross section) into a ribbon that makes an angle of some 30 deg with the endwall. Despite these effects, many critical features of the vortex are almost unaffected by the endwall motion. The vortex produces almost the same magnitude of streamwise mean-velocity deficit, and this deficit still dominates both the mean velocity field and the production of turbulence. Thus, although endwall motion distorts and displaces the leakage vortex it does not fundamentally alter the mechanisms that govern the development of its mean flow and turbulence structure.

Introduction

CONSIDER the blades of a core compressor, an aircraft engine fan, or a marine propulsion pump. As the blades rotate and generate lift, vorticity is shed from their tips and becomes embedded in, and can come to dominate, the casing boundary layer. Accurate prediction of this vortical component of the blade wakes as it evolves downstream of the blade row is important in characterizing its interaction with downstream elements, such as a stator row, and thus predicting aerodynamic performance and the production of noise and vibration. Developing such prediction methods requires detailed experimental information about the mean flow and turbulence structure of the leakage flow and its streamwise evolution. Providing that information, and related physical understanding, is the overall goal of this study.

Given that the tip gaps of most turbomachinery blade rows are fairly small (on the order of 1% chord for a compressor or fan and 3% for a propulsion pump), it seems likely that the relative motion between the blade tips and casing, referred to here as *endwall motion*, will be an important factor, perhaps the most important factor, in determining the structure and development of the leakage flow. However, the effects of endwall motion are poorly understood, partly because it is often difficult to separate this factor from others such as blade loading and centrifugal effects.

One of the first cascade studies concerned with tip-gap effects in compressors set out to examine the effect of endwall motion on the leakage flow for various tip gaps up to 10% chord. Dean[1] measured blade loading and stagnation pressure distributions at the exit of a linear cascade producing 25 deg of turning, with a relatively thick inlet boundary layer (36% chord). The endwall of this cascade was formed from a gritless sanding belt that could be driven at varying speed to simulate the motion of the blade tips past the casing. Unfortunately all of these speeds were all significantly greater that the pitchwise component of the cascade inlet velocity, this being the needed velocity for the system to correctly model a compressor rotor. The belt extended from the trailing-edge line to some 40% chord upstream of the cascade, producing some inlet skew in the oncoming boundary layer. Dean found that the wall motion significantly increased the loading on the tip, over a region that extended at least 9% chord from the tip. His stagnation pressure measurements show a high loss region, which he terms the "boundary-layer heap," adjacent to the endwall at the cascade exit. This region, which seems likely to have contained the tip-leakage vortex, is seen to be moved significantly across the passage toward the pressure side in the presence of wall motion. This same region increases in size with tip gap.

An alternative approach to modeling endwall motion was used by Doukelis et al.,[2,3] who performed measurements on the flow through an annular compressor cascade. The cascade consisted of 19 stationary blades arranged around a rotating hub, from which they were separated by a range of tip gaps between 0.2 and 5.5% chord. The relative motion of the hub and inner blade tips was used to simulate the relative motion of the tips and casing. With a nonuniform swirling inflow (swirl is required for the blades to work like those of a compressor) and a boundary-layer 20% chord in thickness, Doukelis et al. measured blade loading and used impact probes and laser Doppler anemometry to measure stagnation pressure, mean velocities, and some turbulence intensities in the cascade. Their measurements, like those of Dean, show that wall motion significantly increases the tip loading. Reminiscent of the results if Inoue and Kuroumaru,[4] measurements made adjacent to the hub show the track of the developing tip-leakage vortex as a strip of high turbulence levels that grows across the passage.

Dean's[1] observation that the endwall motion influences the penetration of the leakage flow into the passage is perhaps explained by the fact that in compressor configurations the endwall motion and leakage flow through the tip gap are in the same direction. One would therefore expect the viscous shear produced by the endwall to assist the leakage flow. Circumstantial evidence for this effect was provided by Lakshminaryana et al.,[5] who compared mean-velocity measurements on the flow through the blade passages of a compressor rotor and with linear cascade results reported by Lakshminarayana and Horlock.[6] They state that in a cascade without endwall motion the leakage flow rolls into a vortex that stays attached to the suction side of the blade rather than crossing the passage as in a rotor. The statement appears supported by the work of Kang and Hirsch,[7–9] who studied the evolution of the leakage vortex formed in a fairly heavily loaded compressor cascade with stationary endwall for tip gaps between 0 and 3.3% chord. At 2% tip gap their mean-flow measurements show a round tip-leakage vortex forming near the suction side of the blade leading edge but remaining

Received 17 September 2003; revision received 18 June 2004; accepted for publication 23 June 2004.

*Graduate Assistant, Department of Aerospace and Ocean Engineering, 215 Randolph Hall. Student Member AIAA.

†Professor, Department of Aerospace and Ocean Engineering, 215 Randolph Hall. Senior Member AIAA.

attached to the suction side of the blade tip. Like Lakshminarayana and coworkers, they attribute this result to the lack of relative motion between blade tip and endwall.

Whether or not this is the case, our own results suggest that the picture is more complex. In Part 1 of this study,[10] measurements were presented for a linear cascade without endwall motion, but with similar loading and tip characteristics to those of the rotor flow studied by Inoue and coworkers.[4,11] Oil-flow visualizations within the blade row, and velocity measurements downstream, show quite close similarity between the two tip-leakage flows. In particular, the footprint of the cascade leakage vortex on the endwall was seen to leave the blade suction surface at about 20% chord station and cross the blade passage, much like that observed in the rotor flow. It seems likely therefore that other factors, such as blade loading, are at least as important in determining the trajectory of the vortex.

The purpose of this paper is to provide measurements of the tip-leakage flow downstream of a linear cascade that reveal unambiguously the effects of endwall motion. The measurements reveal, for the first time, the exclusive effects of endwall motion on the turbulence structure of the vortex and its development downstream of a blade row. Our approach, like that of Dean,[1] is to use the belt system to produce relative motion between the blade tips and endwall and to use hot-wire anemometry to document its effects on the flow. More details of the apparatus, instrumentation, and results presented next are reported by Wang.[12]

Apparatus and Instrumentation

Measurements were made in the same eight-blade linear cascade facility described in Part 1 (Ref. 10) and using the same three-component hot-wire instrumentation and procedures. We therefore describe here only the modifications to the facility associated with the moving endwall system and the instrumentation used to monitor and evaluate its performance. The cascade parameters are as follows: inlet angle 65.1 deg, stagger angle 56.9 deg, turning angle 12.5 deg, solidity 1.076, blade chord 254 mm, axial chord 139 mm, blade span 254 mm less tip gap, and tip gaps of 0.8, 1.6, and 3.3% chord.

Moving Endwall System

Figure 1 shows a plan view of the moving endwall system installed in the cascade tunnel. Figure 2 shows the system as seen in a cross section through the blade row. In essence, the system consists of a 686-mm-wide belt that slides over the lower endwall of the cascade, beneath the tips of the cantilevered blades. To correctly simulate the relative motion between the blades of a rotor and its casing, the belt must move in the pitchwise direction at a speed equal to the pitchwise component of the inlet velocity. With a nominal freestream velocity of 26 m/s and an inlet angle of 65.1 deg, the belt speed is 23.6 m/s.

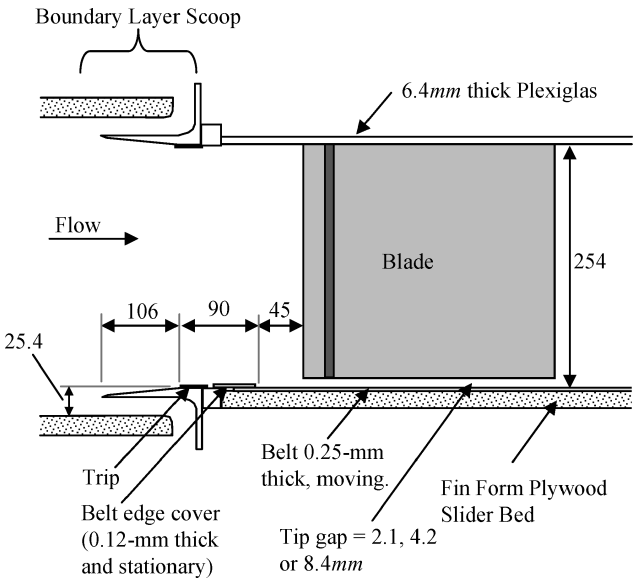

Fig. 2 Cross section through the cascade taken along the inlet flow direction; dimensions in millimeters.

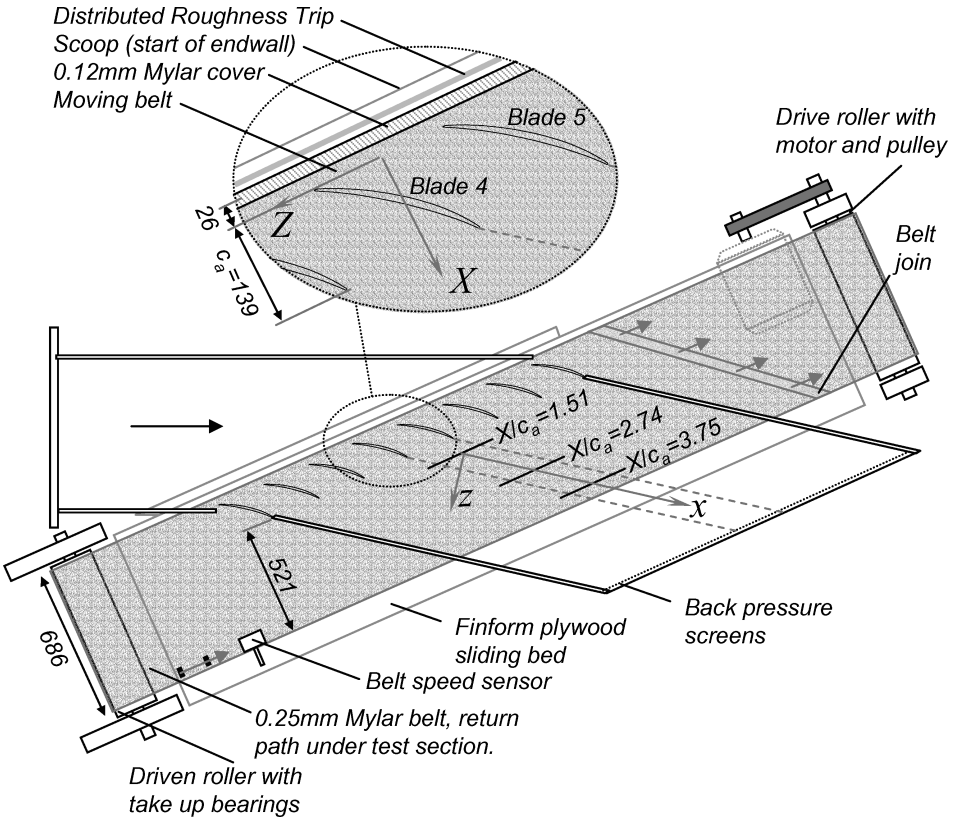

Fig. 1 Plan view of the cascade wind tunnel showing the moving endwall system, coordinate systems, and measurement locations; all dimensions in millimeters.

This motion was generated by roller system consisting of two 203-mm-diam, 762-mm-wide rollers built and dynamically balanced to 2000 rpm by Timesavers, Inc. The two rollers are positioned 3.76 m apart on either side of the blade row, with their axes horizontal and their tops level with the lower endwall of the cascade. The rubber-lagged drive roller, turned by pulley from a 15-hp ac synchronous motor, is used to pull the belt across the endwall and return it beneath the tunnel structure. The unlagged driven roller, located on the opposite side of the cascade, is mounted on take-up bearings. The position of these bearings can be adjusted to alter the tension in the belt and the angle of the roller, which control the tracking of the belt. Accurate tracking is assisted by a slight crown in the driven roller. The speed of the belt is varied using a TOSHIBA® Tosvert-130G2+ digital variable-frequency controller connected to the motor.

Because of the high speeds required, we opted for a belt fabricated from 0.25-mm-thick Mylar film. This kind of film is light, has a high tensile strength, and low flexibility under tension—important for tracking at speed. It is inexpensive so that belts can be frequently replaced, and it is easily joined to form a continuous loop after installation on the roller system. We used a 38-mm-wide lap joint welded together using a soldering iron at several hundred points (Fig. 1). The overlap (occupying about 0.5% of the total belt length) produces a step of close to 0.3 mm in height.

Although the roller system was mounted independently of the tunnel to prevent the transmission of any vibration, some small modifications to the facility were necessary to accommodate it. In its nominal operating position, the belt covered not only the lower endwall beneath the cascade blade tips, but also a 26-mm-wide margin upstream and a 521-mm wide margin downstream (Fig. 1). The aluminum plate, which served as the lower endwall for the work presented in Part 1 (Ref. 10), was replaced with Finform plywood. The polished epoxy finish of the plywood served as a better sliding surface for the Mylar belt. To allow the belt to enter and exit the test section, a 6-mm-high gap was cut out of the bottom of the tailboards forming the test-section sides. Flow through these gaps did not appear to have any significant effect on the pressure rise or turning angle produced by the cascade.

The positive pressure difference between the inside of the test section and the laboratory (produced by the backpressure screens at the tunnel exit) was used to hold the belt on the endwall. For this purpose the endwall was perforated beneath the belt with numerous small holes arranged in streamwise grooves. However, initial tests showed that only those holes closest to the sidewall where the belt entered the test section were necessary, and thus all others were blocked. These holes alone appeared to remove all of the air from between the belt and sliding surface. To prevent air from subsequently getting under the windward edge of the belt (upstream of the cascade) and destroying this vacuum effect, the edge was covered using a 38-mm-wide strip of 0.12-mm-thick Mylar attached to the stationary endwall upstream (see Figs. 1 and 2).

With the exception of the belt and this cover, the endwall geometry, including boundary-layer trip, was identical to that used with the stationary endwall tests reported in Part 1. Measured along the inlet flow direction, the endwall boundary layer grew over 135 mm of endwall from the boundary-layer trip to the cascade leading-edge line, of which the last 45 mm was in motion (see Fig. 2). Inflow boundary-layer measurements made at the cascade leading-edge line close to the center of the central passage (formed by blades 4 and 5) showed a boundary-layer thickness of 6.5 mm (close to the 5.6 mm measured before installation of the moving belt system[10]). Although inflow boundary-layer measurements were not made with wall motion, it seems certain (given the short section of moving endwall ahead of the cascade) that the boundary-layer thickness at the cascade entrance would have been almost the same.

Moving Endwall Instrumentation and Characteristics

To operate the belt at the correct component of the cascade inlet velocity required continuous monitoring of the belt speed. Belt speed was measured directly (to eliminate any errors from slippage on the rollers) using an optical system located outside of the test section, adjacent to the driven roller (see Fig. 1). A sensor module, consisting of an infrared light-emitting diode, an infrared photodiode, and operating circuitry, was suspended above the leeward edge of the belt. Two small ($6 \times 38 \times 1$ mm thick) plastic mirrors were attached to the top surface of the belt adjacent to its leeward edge and separated by a measured distance (about 100 mm). The passage of the mirrors under the sensor module produced two spikes in the photodiode output used to start and stop a digital clock and thus provide a measurement of the belt speed once per revolution. A digital display was used to monitor the time and thus belt speed. With this system we found it possible to set the belt speed to a desired value and hold the speed constant, to within a fraction of a percent, over the course of a measurement.

Before making flow measurements with the moving endwall system in operation, its vibration and thermal characteristics were studied. We attempted to measure the amplitude of vibration by taking a sequence of short exposure (0.002s) photographs[12] of the optically magnified image of the tip of one of the center blades (blade 5) and its reflection in the belt. Taken at a glancing angle to the belt, such photographs should reveal vertical motion of the belt through vertical motion of the reflection. Averaging measurements from some 30 photographs, the rms amplitude of vibration was estimated at 0.05 mm, equivalent to about 2.6% of smallest tip gap studied. However, because this figure is roughly equal to the uncertainty of the measurement technique it only represents only an upper limit on the true vibration amplitude. The physical reason for the low vibration is that, with limited suction where it enters the tunnel, the motion of the belt is very effective at removing any air between it and the sliding surface. Indeed the resulting vacuum appeared to hold the Mylar tighter to the sliding surface than when it was stationary.

With the close contact between the belt and sliding surface, we were concerned about frictional heating of the belt and thus the formation of a thermal boundary layer inside the tunnel flow that would interfere with hot-wire measurements. To address this concern, temperatures were measured using a thermocouple mounted 2.5 mm above the belt (roughly the closest distance at which hot-wire measurements were made) and a second thermocouple in the potential core of the flow during start up and extended running of the belt. Both thermocouples were positioned 150 mm upstream of the leeward side of the belt downstream of the center passage of the cascade. The temperature measured by the near-wall thermocouple was consistently higher than that measured in the potential core but only by 0.1–0.2°F (0.05–0.1°C), a difference insufficient to produce significant error in hot-wire measurements.

Results and Discussion

Results are presented using the blade-row aligned coordinate system (X, y, Z) used to define positions and the outflow aligned system (x, y, z) used to define the mean and fluctuating velocity components (U, V, W) and (u, v, w) (see Fig. 1). The origin of the (X, y, Z) system is at the endwall, midway between the leading edges of blades 4 and 5 that frame the center cascade passage. Distances are normalized on the total blade chord c of 254 mm or its axial (X-wise) component c_a of 139 mm. Velocities are normalized on the inlet velocity in the potential core upstream of the cascade U_∞, which for the tests here was 25.8 ± 0.04 m/s, giving a chord Reynolds number $U_\infty c/\nu$ of $3.90 \times 10^5 \pm 2.5 \times 10^3$. Most measurements were made for a tip-gap-to-chord ratio $t/c = 1.6\%$, equivalent to 40% of the maximum blade thickness and 70% of the inlet boundary-layer thickness. This tip gap is referred to as the baseline case. Measurements were also made for $t/c = 0.8$ and 3.3%.

The flow structure downstream of the central passage of the cascade was documented by making three-component velocity and turbulence measurements over cross-sectional (Y, Z) planes. Measurements were made at $X/c_a = 1.51$, 2.74, and 3.75 (see Fig. 1) in the baseline case and at $X/c_a = 2.74$ in the flows produced with smaller and larger tip gaps. At each station measurements were first made with the belt stationary and then with it moving. This strategy was designed to minimize the uncertainty in comparisons showing the effects of endwall motion. The stationary endwall measurements at $X/c_a = 2.74$ and 3.75 essentially duplicate those presented in Part 1 for $X/c_a = 2.83$ and 3.77 and so are not presented here.

Table 1 Uncertainty estimates at 20:1 odds estimated using the method of Kline and McClintock[13] for the moving endwall measurements[a]

Quantity	Uncertainty
U, V, W	$0.015U_\infty$
$\overline{u^2}$	$0.0004U_\infty^2$
k	$0.0005U_\infty^2$
Ω_x	$0.3U_\infty/c_a$

[a]Uncertainties for stationary endwall results are given in Table 1 of Part 1 (Ref. 10).

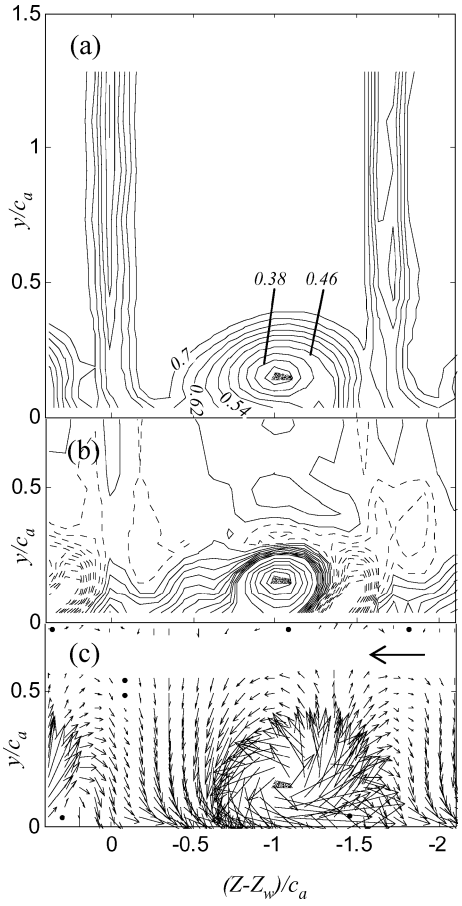

Fig. 3 Flow properties at $X/c_a = 1.51$ for the 1.6%-chord tip gap without endwall motion: a) contours of U/U_∞ in steps of 0.04; b) contours of $\Omega_x c_a/U_\infty$ in intervals of 0.1 from −1 to 1 and intervals of 0.5 from 1.5 to 4 (negative levels are shown dashed); and c) vectors of mean crossflow velocity (V, W). Reference vector of $0.1U_\infty$ in length. Gray shading shows region where $H > 0.9$.

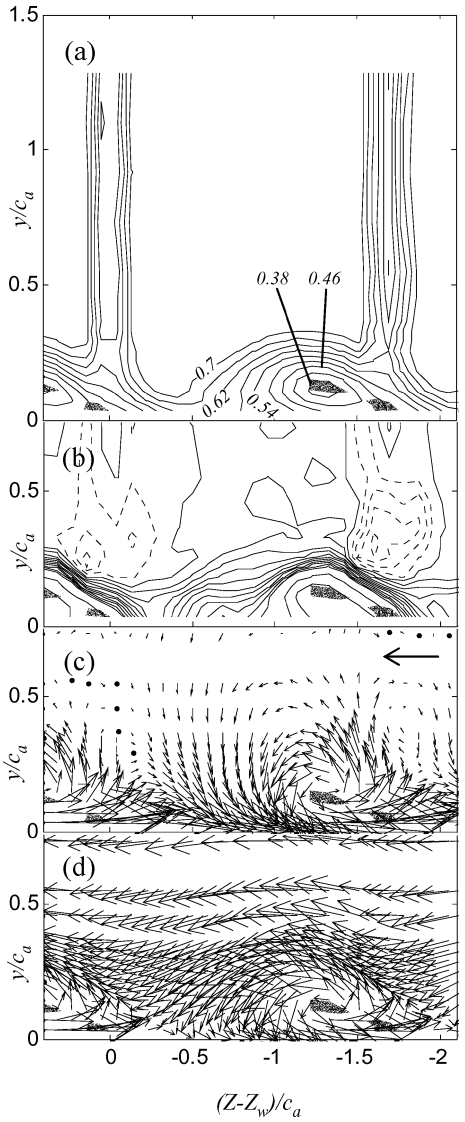

Fig. 4 Flow properties at $X/c_a = 1.51$ for the 1.6%-chord tip gap with endwall motion: a) contours of U/U_∞ in steps of 0.04; b) contours of $\Omega_x c_a/U_\infty$ in intervals of 0.1 from −1 to 1 and intervals of 0.5 from 1.5 to 4 (negative levels are shown dashed); c) vectors of mean crossflow velocity (V, W) (reference vector is $0.1U_\infty$ in length); and d) mean-velocity vectors projected in a plane perpendicular to the vortex trajectory (Fig. 1): Gray shading shows region where $H > 0.9$.

With the belt stationary statistical flow properties (mean velocities, Reynolds stresses, triple products) were determined at each point from 30 records of 1000 samples taken at a rate of 2 kHz over a total measurement time of about 1 min. With it moving, half as many records were taken over about half the measurement time. The shorter measurement time was dictated by the added difficulty of running the belt. Uncertainties in measurements are listed in Table 1.[13]

Effects of Wall Motion Flow Just Downstream of the Cascade

Figures 3 and 4 show the mean-velocity fields measured at $X/c_a = 1.51$ for the baseline case, with and without wall motion. Contours of mean streamwise velocity U/U_∞ and vorticity $\Omega_x = \partial W/\partial y - \partial V/\partial z$ normalized on U_∞ and c_a are shown as well as mean crossflow velocity vectors ($\boldsymbol{V}$, $\boldsymbol{W}$). Vorticity was calculated by numerical differentiation of the mean-velocity data, assuming streamwise derivatives (in x) to be negligible. The aspect ratio of the plots has been adjusted so as to reveal the flow as it would appear if viewed looking upstream along the x axis. Pitchwise locations are shown relative to the center of the wake of blade 4 (at $Z = Z_w$). Vectors are plotted at the measurement locations and thus show the density of the measurement grid.

Without wall motion (Fig. 3) the mean flowfield appears quantitatively consistent with an interpolation of the measurements presented for $X/c_a = 1.37$ and 2.06 in Part 1 (Ref. 10). The vertical wakes of the center passage blades, the potential core between them and the viscous endwall region containing the tip-leakage vortex shed from blade 4, are most clearly visible in the U/U_∞ contours. The vertical wake of blade 4 is to the left of the figure. The vortex is dominated by a large elliptical region of streamwise mean-velocity deficit adjacent to the lower endwall. The maximum deficit (some 40% of the inlet velocity) is roughly twice the maximum mean crossflow velocity produced by the rotating motion of the vortex and twice the streamwise mean velocity deficit seen in the two-dimensional parts of the blade wakes. The secondary flowfield of the vortex shows an elliptical region of rotating flow centered closely on the points of maximum mean streamwise velocity deficit and mean streamwise vorticity. This well-defined center, of peak vorticity $3.5U_\infty/c_a$, is

surrounded by roughly circular vorticity contours. A region of negative vorticity is seen to the right of this vortex core in the region where the rotating motion of the vortex is lifting fluid away from the endwall. Results presented in Part 1 (Ref. 10) suggest that the negative vorticity is associated with a remnant of a secondary structure formed in the blade passage.

Wall motion (Fig. 4) clearly has a substantial impact on the mean flow structure of the endwall region, much as one might expect from earlier studies. The area of mean streamwise velocity deficit produced by the leakage vortex appears flattened by the motion. The maximum velocity deficit occurs closer to the endwall (near $y/c_a = 0.12$ rather than 0.16) and farther to the right (at $Z - Z_w/c_a = -1.29$ rather than -1.02) as though dragged by the pitchwise movement of the endwall. This shift, when compared to the blade spacing appears similar in size to that observed by Dean[1] at his lowest wall speed. In addition, the entire lower half of its streamwise velocity distribution appears sheared by the endwall motion. Consistent with this, the secondary flow vectors of Fig. 4c show a significant layer of fluid (0.1 to $0.2c_a$ thick) adjacent to the endwall being pulled to the right by the endwall. This flow both deforms and, to some extent, obscures the secondary velocity field generated by the vortex. Perhaps the largest effects are seen in the contours of streamwise mean vorticity (Fig. 4b). The peak vorticity is significantly lower than without wall motion ($2U_\infty/c_a$ instead of $3.5U_\infty/c_a$) and occurs much closer to the endwall. Furthermore, the distribution of vorticity around the peak is completely altered, from the vortex centered field seen without wall motion to one in which the vortex appears as just one component of a vortex sheet produced between the potential core and moving endwall.

Despite these changes, some important features of the mean flowfield are unaffected by the endwall motion. The vortex still produces a large streamwise mean-velocity deficit, about $36\%U_\infty$ at maximum, and a relatively weak tangential velocity field. The maximum mean tangential velocity produced by the vortex is harder to judge from the vectors of Fig. 4c because of the superimposed flow across the endwall. The tangential velocities of the vortex are more easily seen if the vectors are projected into a plane perpendicular to the trajectory of the vortex, as shown in Fig. 4d. Trajectory was inferred from additional measurements made downstream, to be presented next. Here the rotating flowfield is seen to have a roughly elliptical form with a peak tangential velocity of about $16\%U_\infty$, somewhat less the value of close to 20% indicated by the stationary endwall data of Fig. 3c. The dominance of the streamwise velocity field suggests that the gradients of this component are likely to be the major turbulence producers, just as without wall motion.

One difficulty in analyzing the flow in the presence of endwall motion is that of defining the vortex center. The streamwise vorticity distribution simply does not show a peak in the vortex (used to define the center of the stationary endwall vortices in Part 1), and the region of largest vorticity does not in any case appear coincident with that of maximum streamwise velocity deficit. In an attempt to unambiguously define the center, we have plotted on top of the distributions shown in Figs. 3 and 4 shaded regions where the normalized mean-helicity density H exceeds 0.9. Helicity density, defined as $\boldsymbol{\Omega}.\boldsymbol{V}/|\boldsymbol{\Omega}||\boldsymbol{V}|$, where $\boldsymbol{\Omega}$ and $\boldsymbol{V}$ are respectively the mean vorticity and velocity vectors, reaches 1 or -1 at the center of a streamwise mean vortex. Without wall motion (Fig. 3) the small region defined by $H > 0.9$ identifies the vortex center as being right at the peak of the streamwise mean vorticity distribution and the center of the coincident streamwise velocity deficit and rotating secondary flowfield. With wall motion (Fig. 3) $H > 0.9$ actually defines two more elongated regions, one at the center of the streamwise mean velocity deficit and the other adjacent to the endwall to the right of this point. Interestingly, neither of these is centered on the area of greatest streamwise mean vorticity. The spatial resolution of the measurements is not really sufficient to distinguish whether these two regions are distinct or part of a single strip. However, results from farther downstream (where the vortex is bigger and the effective measurement resolution better) clearly support the latter interpretation. We therefore conclude that with wall motion the tip-leakage vortex does not have a point center. Instead, the wall motion

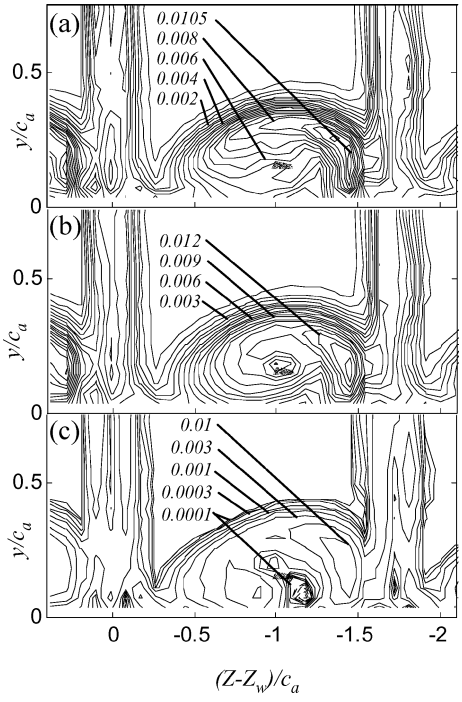

Fig. 5 Flow properties at $X/c_a = 1.51$ for the 1.6%-chord tip gap without endwall motion: a) contours of u^2/U_∞^2 in intervals of 0.0005; b) contours of k/U_∞^2 in intervals of 0.00075; and c) contours of turbulence-kinetic-energy production Negative levels are shown dashed. Gray shading shows region where $H > 0.9$.

distributes the center into a ribbon that, in this particular case, makes an angle of some 30 deg with the endwall.

One can ask whether a structure without a point center is really a vortex at all. Indeed the present conclusion is somewhat reminiscent of the observations of Lakshminarayana et al.[14] who, for flow through the passage of a compressor rotor, describe the leakage flow as an overturning jet rather than the vortex. However, in the present case the leakage flow clearly produces an organized rotating cross-flow field (Fig. 4d). We therefore feel that the term vortex is still appropriate.

The turbulence structure of the two vortices at $X/c_a = 1.51$ is compared in Figs. 5 and 6 in terms of contours of turbulence normal stress $\overline{u^2}/U_\infty^2$, turbulence kinetic energy $k/U_\infty^2 = \frac{1}{2}(\overline{u^2} + \overline{v^2} + \overline{w^2})/U_\infty^2$, and turbulence-kinetic-energy production normalized on U_∞ and c_a. The production was computed by finite difference ignoring streamwise derivatives $\partial/\partial x$. Without endwall motion (Fig. 5) turbulent activity in the vortex is concentrated in an arc-shaped region that circles the top and right-hand sides of the vortex center. The k/U_∞^2 and $\overline{u^2}/U_\infty^2$ reach peak levels of 0.0135 and 0.0105 in this region respectively (a turbulence intensity of about 14%, based on the local velocity of the potential core). At the vortex center itself the turbulence stresses are some 30% lower than these peak values. Although this could be partly a consequence of the stabilizing effects of rotation, the main reason is actually that the streamwise mean velocity gradients (Fig. 3a) are smaller near the vortex center, and it is these gradients that are the dominant contributors to the turbulence production. The turbulence production

$$-\overline{uv}\frac{\partial U}{\partial y} - \overline{uw}\frac{\partial U}{\partial z} - \overline{v^2}\frac{\partial V}{\partial y} - \overline{w^2}\frac{\partial W}{\partial z} - \overline{vw}\left(\frac{\partial V}{\partial z} + \frac{\partial W}{\partial y}\right)$$

for this case is plotted in Fig. 5c. The arc of turbulent activity is most pronounced and complete in the production distribution, as is the reduced turbulent activity in the vicinity of the vortex center, where production actually becomes negative. Separating the production into its component terms and integrating their net contribution over the measured cross section, we find that the first two terms (associated with gradients in the streamwise mean velocity) are by far the

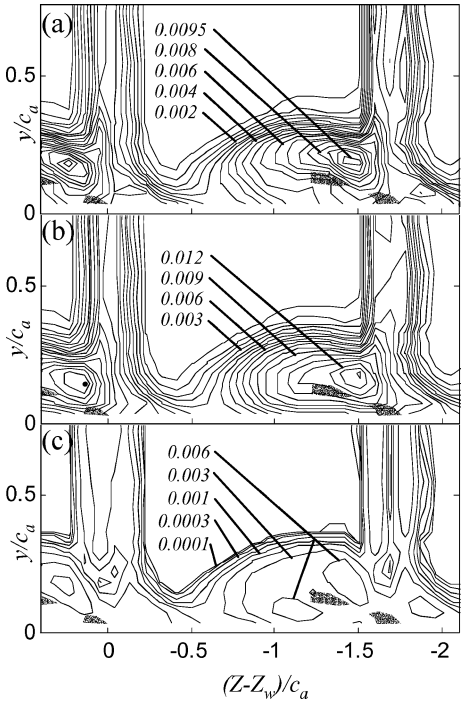

Fig. 6 Flow properties at $X/c_a = 1.51$ for the 1.6%-chord tip gap with endwall motion: a) contours of $\overline{u^2}/U_\infty^2$ in intervals of 0.0005; b) contours of k/U_∞^2 in intervals of 0.00075; and c) contours of turbulence-kinetic-energy production. Gray shading shows region where $H > 0.9$.

largest contributors to the production, accounting for some 74% of the total.

With wall motion (Fig. 6) the distributions of the turbulence properties show the same shift to the right and flattening of the vortex seen in the mean-velocity measurements. Despite this, the region of high turbulence levels above the vortex persists. The region contracts somewhat and loses some of its curved shape. Indeed, with wall motion this region is more like a band lying just above ribbon of large helicity defining the vortex center. Peak turbulence levels, reached in the band near its center at $(Z - Z_w)/c_a = -1.5$, are quite close to those measured without wall motion, at 0.0135 for k/U_∞^2 and 0.0095 for $\overline{u^2}/U_\infty^2$. The balance of normal stresses (not pictured) is also similar to the stationary wall case and with Puddu's[15] observations in a fan tip wake. Stresses $\overline{u^2}$ and $\overline{w^2}$ are on average 10 to 20% larger than $\overline{v^2}$. The shear stress $\overline{uw}$ is particularly dominant close to the endwall.

Turbulence-kinetic-energy production (Fig. 6c) becomes concentrated in two bands with endwall motion, one below and one above the vortex-center ribbon. Peak production levels are about 40% lower with wall motion, but the terms dominating the production are the same. Streamwise mean-velocity gradients, which have a distribution (Fig. 4a) that closely mirrors the production, are responsible for about 67% of the total production in the cross section. Contributions to the production from secondary flow velocity gradients are slightly larger with wall motion primarily because the term $-\overline{vw}(\partial W/\partial y)$ is elevated in the near-wall region because of pitchwise shear between cascade outflow and the moving endwall.

To summarize, we see that while endwall motion distorts the leakage vortex, stretching its center into a ribbon and dragging it across the endwall, it does not fundamentally alter the mechanisms that govern its development. It is still dominated by its streamwise mean-velocity deficit and the turbulence it produces.

Development of the Flow with Downstream Distance

The streamwise development of the baseline flow with endwall motion, from $X/c_a = 1.51$ to 2.74 and 3.75, is illustrated in Figs. 7–10 in terms of cross sections of U, Ω_x, k, and production of k, normalized as appropriate on U_∞ and c_a. Overlaid on these pictures are shaded areas of $H > 0.9$ identifying the vortex center regions.

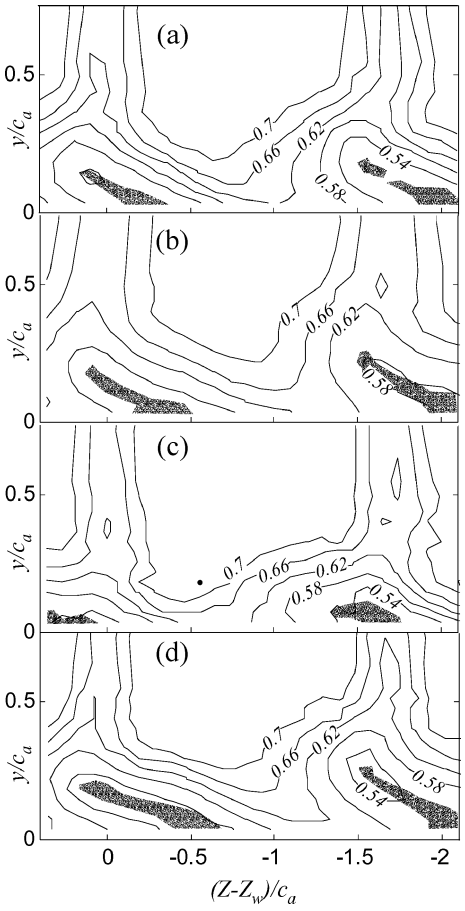

Fig. 7 Contours of U/U_∞ in steps of 0.04 with endwall motion: a) tip gap 1.6% chord, $X/c_a = 2.74$; b) tip gap 1.6% chord, $X/c_a = 3.75$; c) tip gap 0.8% chord, $X/c_a = 2.74$; and d) tip gap 3.3% chord, $X/c_a = 2.74$. Gray shading shows vortex center regions where $H > 0.9$.

The ribbonlike structure of the vortex center becomes more apparent with at these downstream stations. In the projection shown, the ribbon is a little over half an axial chord in width and sits at an angle of close to 30 deg to the endwall. Figure 11 compares the trajectory of the ribbon with that of the vortex center seen without wall motion. The figure also shows the location of the center of the two-dimensional wake of the blade shedding the vortex (blade 4) and the cascade outlet angle. This figure reveals that wall motion shifts the pitchwise position of the vortex center by an almost constant distance (about $0.5c_a$), so that the trajectories with and without wall motion are almost parallel. The implication is that the shift in position occurs upstream of the measured part of the flow and is not connected with any difference in vortex strength or mechanism within in the measured length.

If anything, the vortex center ribbon becomes more closely associated with the streamwise mean-velocity field with distance downstream (Figs. 7a and 7b). At $X/c_a = 2.74$ and 3.75 the center ribbon becomes almost perfectly aligned with the region of greatest deficit. This is despite the fact that the peak deficit itself weakens with downstream distance, from 36% U_∞ at $X/c_a = 1.51$ to 20% U_∞ and then 16% U_∞ at $X/c_a = 2.74$ and 3.75, and that the vortex grows over this distance and moves beneath the wake shed by the adjacent blade. Note that this decay of the streamwise velocity deficit magnitude quite closely follows that of the vortex without endwall motion.

The streamwise velocity field continues to control the turbulence structure and production with distance downstream. Turbulence kinetic energy remains greatest in the band above and to the right of the center ribbon where the streamwise velocity gradients are largest. Peak turbulence kinetic energy in this region decays from 0.0136 U_∞^2 at $X/c_a = 1.51$ to 0.0050 U_∞^2 at $X/c_a = 3.75$, a little slower than the rate of decay in the two-dimensional portions of the

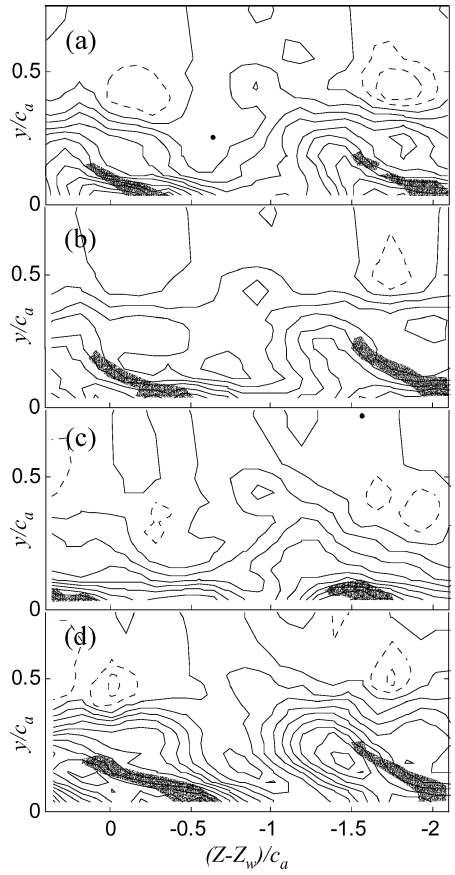

Fig. 8 Contours of $\Omega_x c_a/U_\infty$ in intervals of 0.1 from −1 to 1 and intervals of 0.5 from 1.5 to 4, with endwall motion. Negative levels are shown dashed: a) tip gap 1.6% chord, $X/c_a = 2.74$; b) tip gap 1.6% chord, $X/c_a = 3.75$; c) tip gap 0.8% chord, $X/c_a = 2.74$; and d) tip gap 3.3% chord, $X/c_a = 2.74$. Gray shading shows vortex center regions where $H > 0.9$.

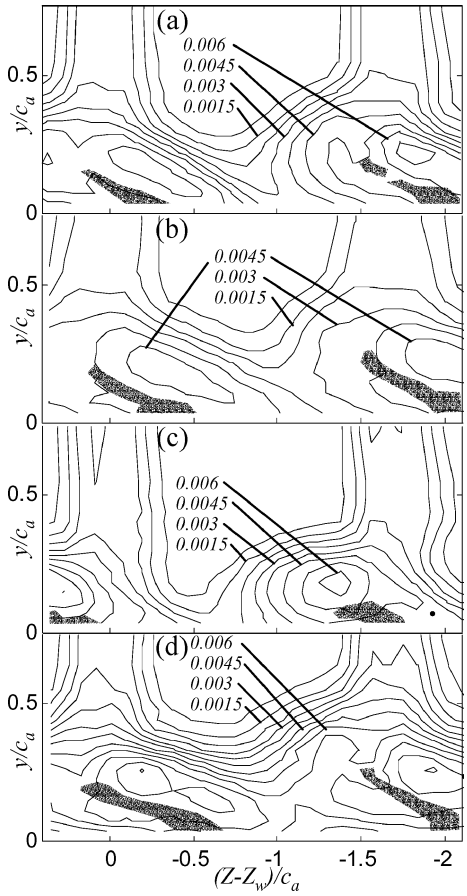

Fig. 9 Contours of k/U_∞^2 in intervals of 0.00075, with endwall motion: a) tip gap 1.6% chord, $X/c_a = 2.74$; b) tip gap 1.6% chord, $X/c_a = 3.75$; c) tip gap 0.8% chord, $X/c_a = 2.74$; and d) tip gap 3.3% chord, $X/c_a = 2.74$. Gray shading shows vortex center regions where $H > 0.9$.

blade wakes away from the endwall (see Part 1,[10] Fig. 13). Interestingly these peak levels are also close to those seen in the same baseline vortex without wall motion (see Part 1, Fig. 13). Production of turbulence kinetic energy in the moving endwall vortex remains largest in bands that lie both above and below the center. Production remains dominated by terms associated with gradients of U, though not quite to the extent seen in the stationary endwall flow. When integrated over the cross section, these terms account for 77 and 83% of the total production at $X/c_a = 2.74$ and 3.75, respectively.

Curiously uncoupled from this structure and its development is the secondary flow velocity field represented in Fig. 8 by the mean streamwise vorticity. At both $X/c_a = 2.74$ and 3.75 a tongue of elevated vorticity levels is seen extending from the endwall with roughly the same shape and orientation as the vortex center ribbon. However, the tongue is simply in different place, below and to the left of the center. This rather striking disconnect can be partly explained by the fact that the relative motion of the endwall and cascade outflow must produce a layer of streamwise vorticity in the endwall boundary layer, with the same sense of the vortex. The gradient of vorticity across this layer is visible between the endwall vortices in Figs. 8a and 8b. Although the vorticity of this layer and that of the leakage vortex would not just be superposed, it is true that adding such a gradient to the vorticity field of the vortex would shift its apparent center (the location of peak vorticity) toward the endwall. As at $X/c_a = 1.51$ peak streamwise vorticity levels in the vortex region are substantially lower (about half) with wall motion, than without (compare with Part 1, Fig. 9).

Effects of Tip Gap

Figures 7–10 include cross sections of the same mean flow and turbulence properties measured at $X/c_a = 2.74$ but with tip gaps of 0.85 and 3.3% chord, one-half and twice that of the baseline flow. Much as seen without wall motion, the tip gap controls both the size and location of the tip-leakage vortex. For $t/c = 0.85\%$ the streamwise mean velocity field (Fig. 7c) shows the influence of the vortex extending to about $0.3c_a$ from the endwall. Increasing the tip gap through 1.65%c (Fig. 4a) to 3.3% (Fig. 7d) roughly doubles the height of this region. At the same time the vortex center ribbon shifts to the right (in the negative Z direction) away from the rest of the wake of blade 4 and becomes longer. The ribbon remains closely associated with the region of greatest streamwise velocity deficit, the peak deficit itself being more or less independent of tip gap, just as in the flow without endwall motion [compare with Fig. 8 of Part 1 (Ref. 10)].

The contours of mean streamwise vorticity show that the strength of the vortex, as measured by the size and intensity of the region of elevated vorticity within it, increases with tip gap. However, the impact of this crossflow velocity field on the rest of the flow remains minimal, and the region of elevated vorticity remains below the true vortex center. Turbulence kinetic energy levels, which increase slightly (about 25%) with tip gap from $t/c = 1.65$ to 3.3%, still reach their maximum values above the vortex center ribbon where streamwise velocity gradients dominate. Peak turbulence production, which has a similar distribution and peak level for all three tip gaps, is still predominantly the result of U gradient terms. When integrated over the cross section, the proportion of turbulence production as a result of these terms decreases only slowly with tip gap, from 79% for $t/c = 0.85\%$, through 77% for $t/c = 1.6\%$ to 69% for $t/c = 3.3\%$.

In summary then we find that tip gap does not qualitatively influence the vortex structure or the mechanisms that drive it in the presence of wall motion. Comparing these results with those of Figs. 8–11 of Part 1 (Ref. 10), we see that, just as in the baseline case, the peak streamwise mean-velocity deficit and peak turbulence

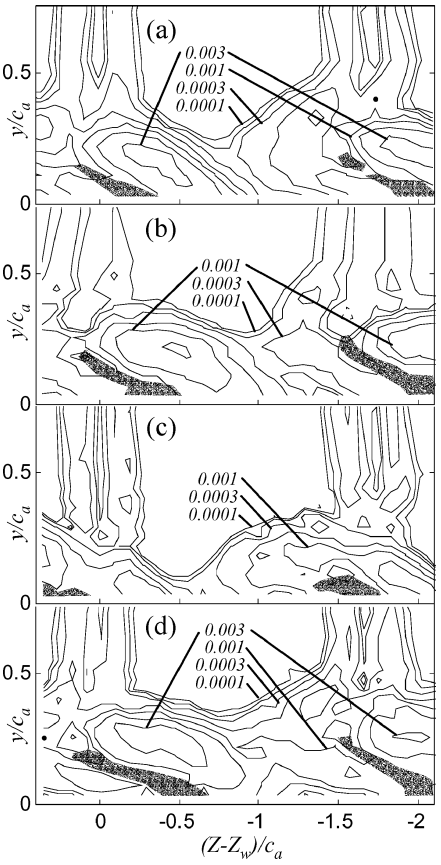

Fig. 10 Contours of turbulence kinetic energy with endwall motion. Contour levels are 0.0001, 0.00017, 0.0003, 0.0006, 0.001, 0.0017, and 0.003: a) tip gap 1.6% chord, $X/c_a = 2.74$; b) tip gap 1.6% chord, $X/c_a = 3.75$; c) tip gap 0.8% chord, $X/c_a = 2.74$; and d) tip gap 3.3% chord, $X/c_a = 2.74$. Gray shading shows vortex center regions where $H > 0.9$.

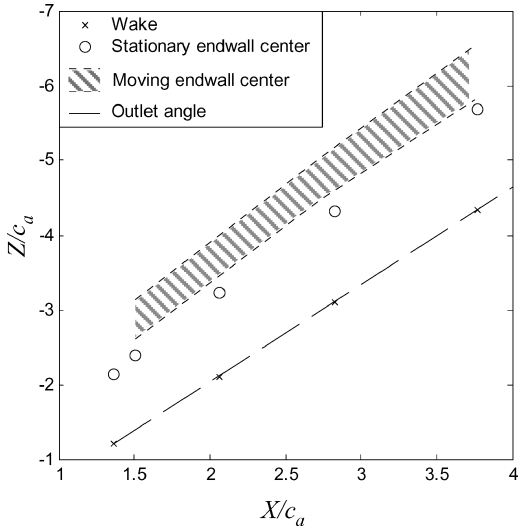

Fig. 11 Comparison of the trajectory of the center of the vortex shed by blade 4, with and without endwall motion, with the wake center trajectory and the outlet angle for a tip gap of 1.6% chord.

kinetic energy in the vortex are not strongly influenced by the wall motion, but wall motion significantly lowers peak streamwise vorticity levels.

Conclusions

The flow downstream of a linear compressor cascade with tip gap has been studied with and without the effects of the relative motion between the blade tips and endwall that would be experienced in a rotor flow. This endwall motion was simulated by using a 0.25-mm-thick Mylar belt propelled over the surface beneath the blade tips. The fluid dynamics of such a belt produces a vacuum between it and the sliding surface that reduces belt vibration to a negligible level.

Three-component mean-velocity and turbulence measurements were made in cross sections at three axial stations ($X/c_a = 1.51$, 2.74, and 3.75) downstream of the cascade trailing edge for a tip gap of 1.65% chord. Measurements for tip gaps of 0.085 and 3.3% chord were also made at $X/c_a = 2.74$. These results reveal some clear effects of endwall motion on the mean flow and turbulence structure of the vortex and its development downstream of a blade row.

Wall motion has a substantial impact on the mean flow structure of the leakage vortex. Turbulence and mean streamwise velocity distributions show the vortex being flattened and sheared by the motion. The 0.1–$0.2c_a$-thick layer of fluid dragged with the pitchwise movement of the endwall also deforms and obscures the mean secondary flow and streamwise vorticity fields of the vortex. Streamwise vorticity levels drop, and the vorticity field loses the clear vortex-centered structure seen without endwall motion. Contours of mean-helicity density show that the endwall motion smears the vortex center from a single point (when seen in cross section) into a ribbon that makes an angle of some 30 deg with the endwall. As the vortex evolves, this ribbon remains centered on the region of greatest streamwise mean velocity deficit in the vortex, rather than the region of greatest streamwise vorticity. The vortex center is also shifted pitchwise by about $0.5c_a$ by the wall motion. This magnitude of this shift does not vary with distance downstream, however, implying that is not connected with any difference in vortex strength or mechanism in the measured length.

Although these effects are certainly significant, it is also true that many critical features of the vortex are almost unaffected by the endwall motion. Wall motion has relatively little effect on the magnitude of the large streamwise mean-velocity deficit at the vortex center and its decay with downstream distance. This streamwise velocity field appears to dominate the much weaker tangential velocity field of the vortex and more or less controls the turbulence structure. Peak turbulence levels in the vortex are also almost the same with and without wall motion. In both cases the highest turbulence levels are experienced in a band above the vortex center where the streamwise mean-velocity gradients are largest. Also in both cases, the production of turbulence kinetic energy within the vortex is dominated by terms associated with streamwise mean-velocity gradients. In short it seems that although endwall motion distorts the leakage vortex, stretching its center and dragging it across the endwall, it does not fundamentally alter the mechanisms that govern its development. It is still dominated by its streamwise mean-velocity deficit and the turbulence it produces.

Changing the tip gap does not qualitatively influence the vortex structure or the mechanisms that drive it in the presence of wall motion. Furthermore increasing tip gap appears to control both the size and location and intensity of the tip-leakage vortex in much the same way, regardless of endwall motion.

Acknowledgments

The authors acknowledge the support of NASA Langley Research Center, in particular Joe Posey, for their support under Grant NAG 1-1801. Some of the analysis of these data was also performed with the support of the Office of Naval Research, under Grant N00014-99-1-0294, administered by Ki-Han Kim. The assistance of Chittiappa Muthanna in setting up the wind tunnel and performing measurements and that of Greg Dudding in building and assembling the belt system is gratefully acknowledged. Numerical results from the experiments described here are available from the authors' Website.‡

References

[1]Dean, R. C., Jr., "The Influence of Tip Clearance on Boundary Layer Flow in a Rectilinear Cascade," Gas Turbine Lab., Rept. 27-3, Massachusetts Inst. of Technology, Cambridge, MA, Dec. 1954.

‡Data available online at http://www.aoe.vt.edu/flowdata [cited 1 Oct. 2004].

[2]Doukelis, A., Mathioudakis, K., and Papailou, K., "The Effect of Tip Clearance Gap Size and Wall Rotation on the Performance of a High-Speed Annular Compressor Cascade," American Society of Mechanical Engineers, Paper 98-GT-38, 1998.

[3]Doukelis, A., Mathioudakis, K., and Papailou, K., "Investigation of the 3D Flow Structure in a High-Speed Annular Compressor Cascade for Tip Clearance Effects," American Society of Mechanical Engineers, Paper 98-GT-39, 1988.

[4]Inoue, M., and Kuroumaru, M., "Structure of a Tip Clearance Flow in an Isolated Axial Compressor Rotor," American Society of Mechanical Engineers, Paper 88-GT-251, 1988.

[5]Lakshminarayana, B., Zhang, J., and Murthy, K. N. S., "The Effects of Tip Clearance on Flow Field and Losses in a Compressor Rotor," *Zeitschrift für Flugwissenschaften und Weltraumforschung*, Vol. 14, No. 4, 1990, pp. 273–281.

[6]Lakshminarayana, B., and Horlock, J. H., "Leakage and Secondary Flows in Compressor Cascades," Aeronautical Research Council, Repts. and Memoranda No. 3483, London, March 1965.

[7]Kang, S., and Hirsch, C., "Experimental Study of the Three-Dimensional Flow Within a Compressor Cascade with Tip Clearance: Part 1—Velocity and Pressure Fields," *Journal of Turbomachinery*, Vol. 115, No. 3, 1993, pp. 435–443.

[8]Kang, S., and Hirsch, C., "Experimental Study of the Three-Dimensional Flow Within a Compressor Cascade with Tip Clearance: Part 2—The Tip-Leakage Vortex," *Journal of Turbomachinery*, Vol. 115, No. 3, 1993, pp. 444–452.

[9]Kang, S., and Hirsch, C., "Tip Leakage Flow in a Linear Compressor Cascade," *Journal of Turbomachinery*, Vol. 116, No. 4, 1994, pp. 657–664.

[10]Muthanna, C., and Devenport, W. J., "Wake of a Compressor Cascade with Tip Gap, Part 1: Mean Flow and Turbulence Structure," *AIAA Journal*, Vol. 42, No. 11, 2004, pp. 2320–2331.

[11]Inoue, M., Kuroumaru, M., and Fukuhara, M., "Behavior of Tip-Leakage Flow Behind an Axial Compressor Rotor," *Journal of Engineering for Gas Turbines and Power*, Vol. 108, No. 1, 1986, pp. 7–14.

[12]Wang, Y., "Tip Leakage Flow Downstream a Compressor Cascade with Moving End Wall," M.S. Thesis, Dept. of Aerospace and Ocean Engineering, Virginia Polytechnic Inst. and State Univ., Blacksburg, VA, URL: http://scholar.lib.vt.edu/theses/available/etd-04052000-14200057/ [cited 5 April 2000].

[13]Kline, S. J., and McClintock, F. A., "Describing Uncertainties in Single Sample Experiments," *Mechanical Engineering*, Vol. 75, No. 1, 1953, p. 3.

[14]Lakshminarayana, B., Pouagare, M., and Davino, R., "Three-Dimensional Flow-Field in the Tip Region of a Compressor Rotor Passage, Part 1: Mean Velocity Profiles and Annulus Wall Boundary Layer," *Journal of Engineering for Power*, Vol. 104, No. 4, 1982, pp. 760–781.

[15]Puddu, P., "Tip Leakage Flow Characteristics Downstream of an Axial Flow Fan," American Society of Mechanical Engineers, Paper 96-GT-508, 1996.

R. So
Associate Editor